



Original article

Endocytosis-associated patterns in nerve regeneration after peripheral nerve injury



Guidong Shi^{a,b}, Dingyu Hao^c, Lei Zhang^c, Jia Qin^c, Guangyuan Tian^c, Boyuan Ma^c, Xianhu Zhou^{d,*}

^a Department of Orthopaedics, Qilu Hospital, Cheeloo College of Medicine, Shandong University, Jinan, Shandong, China

^b Shandong University Centre for Orthopaedics, Cheeloo College of Medicine, Shandong University, Jinan, Shandong, China

^c Department of Orthopaedics, Tianjin Medical University General Hospital, Tianjin, China

^d The Affiliated Hospital of Medical School, Ningbo University, 247 People Road, Jiangbei District, Ningbo, Zhejiang, China

ARTICLE INFO

Keywords:

Peripheral nerve injury
Nerve regeneration
Schwann cells
Demyelination
Endocytosis
Exocytosis

ABSTRACT

Background: Clearance of myelin debris and remyelination of myelin are necessary steps for peripheral nerve remodeling and regeneration. It has yet to be clarified which genes or proteins are involved in endocytosis or exocytosis in the removal of myelin debris during peripheral nerve repair.

Methods: For this project, a rat model of subacute stage of sciatic nerve injury was established first. Subsequently, normal Schwann cells (NSCs) and activated Schwann cells (ASCs) were harvest before and after peripheral nerve injury (PNI). Following methylated DNA immunoprecipitation sequencing (MeDIP-seq) and tandem mass tags (TMT) labeling analysis of NSCs and ASCs, what common biomarkers changes in peripheral nervous systems remain to be elucidated.

Results: A total of 14,770 different expression genes (DEGs) and 3249 different expression proteins (DEPs) were screened between ASCs and NSCs. For the exosomes, the diameter and particles concentration of exosomes were 141.7 nm and 2.97×10^7 particles/mL, respectively. The size distribution of exosomes was 50–200 nm. ASCs showed higher cellular uptake ability than the NSCs by cellular uptake test. Moreover, *RAB7A*, *ARF6*, *ARF1*, *VPS45*, *RAB11A*, *DNM3*, and *NEDD4* were the core markers and may control the molecular mechanism of the Endocytosis pathway.

Conclusion: These biomarkers may play significant roles in the initiation phase of demyelination and axon regeneration.

The translational potential of this article: This study explores that the endocytosis-associated patterns of Schwann cells may be new therapeutic strategy for nerve tissue engineering and nerve regeneration.

1. Introduction

Peripheral nerve injury (PNI) is one of the most common nerve injuries in the world [1–3]. The reasons for peripheral nerve injury are complex and diverse, usually including trauma, infection, compression, ischemia, tumor, and nutritional metabolism disorders [4–6]. After the peripheral nerve injury, Wallerian Degeneration occurs, which activates multiple signaling pathways, inflammation factors, epigenetic regulators [7–9]. Therefore how to promote the survival of neurons, the removal and remodeling of myelin sheaths, the destruction and regeneration of axons are currently accepted treatment options for peripheral nerve repair. At present, the known research and treatment methods mainly

focus on cell repair, drug repair, and multiple factors combined with scaffolds.

After peripheral nerve injury, Schwann cells are released from degenerated nerves, dedifferentiate, and actively participate in axon regeneration [10]. The repair process after peripheral nerve injury includes the phenotypes change of Schwann cell, the reconstruction of the vascular network, and the activation of macrophages [11]. Among them, activated macrophages and dedifferentiated Schwann cells are involve in the removal of myelin debris, forming bumper bands, remyelination and repairing damaged nerves [12]. In addition, the exchange of information and interaction between the dedifferentiated Schwann cells and other cells has become the key to peripheral nerve regeneration, and this exchange of information contains a variety of bioactive components

* Corresponding author.

E-mail address: zhouxh007@126.com (X. Zhou).

<https://doi.org/10.1016/j.jot.2021.09.004>

Received 18 May 2021; Received in revised form 29 August 2021; Accepted 13 September 2021

Abbreviations

NSCs	normal Schwann cells
ASCs	activated Schwann cells
PNI	peripheral nerve injury
MeDIP-seq	methylated DNA immunoprecipitation sequencing
TMT	tandem mass tags
DEGs	different expression genes
DEPs	different expression proteins
qRT-PCR	quantitative real-time polymerase chain reactions
PNI	peripheral nerve injury
FBS	fetal bovine serum
AA	antibiotic-antimycotic
GO	gene ontology
KEGG	Kyoto Encyclopedia of Genes and Genomes

RAB7A	Ras-related protein Rab-7a
ARF6	ADP-ribosylation factor 6
RAB5A	Ras-related protein Rab-5A
RAB11A	Ras-related protein Rab-11 A
RhoA	Transforming protein RhoA
ARF1	ADP-ribosylation factor 1
DNM3	Dynamamin-3
SRC	Proto-oncogene tyrosine-protein kinase Src
NEDD4	E3 ubiquitin-protein ligase NEDD4
VPS45	Vacuolar protein sorting-associated protein 45
BP	biological processes
MF	molecular function
CC	cellular component
Dyn2	dynamamin2

(proteins, lipids, mRNA, lncRNA, and circRNA) [13–15]. In this study, our results indicate that there are many common markers in genome and proteome after peripheral nerve injury, which are involved in the activation and regulation of Schwann cell endocytosis pathway.

Due to the potential inhibitory effect of myelin debris, removal of myelin debris is one of the most important steps in peripheral nerve repair after demyelination [16]. Multiple genes or proteins can promote and regulate the phagocytosis of myelin debris by macrophages and Schwann cells [17–19]. After myelin debris clearance, Schwann cells migrate and aggregate to form myelin sheaths, protect and stimulate repair and regeneration of axons [20]. Therefore, the clearance of myelin debris regulated by the Endocytosis pathway is one of the key factors for axon regeneration.

We here present the endocytosis-related genes and proteins signatures of Schwann cells before and after peripheral nerve injury. This enabled us to deduce the endocytosis-related targets and look for novel way to repair peripheral nerve injury.

2. Materials and methods

2.1. Animals and study design

Eighteen female Wistar rats (250 ± 10 g) aged 8 weeks were obtained from Laboratory Animal Center of Chinese People Liberation Army General Hospital (Beijing, China, Approval Number: SCXK2012-0086). A humidity/temperature-controlled environment with 12-h light/dark cycle and free access to food or water were created for all animals. For ethics, a statement of this project was approved by the Tianjin Medical University General Hospital (Tianjin, China, Approval number: IRB2020-WZ-056). All rats were randomly assigned to two groups as follows: The Sham group (n = 9), which received sciatic nerve exposure only without PNI; The PNI group (n = 9), which the bilateral sciatic nerves were exposed and ligated with silk at the proximal end of the sciatic nerve.

2.2. Isolation and culture of schwann cells

Schwann cells were obtained from the sciatic nerve of Wistar rats according to a previous study [21]. Briefly, all rats were anesthetized with 1% isoflurane to minimize suffering before surgery. After satisfactory anesthesia, the sciatic nerve was ligated in each rat of PNI groups, while the rats in Sham group only received sciatic nerve exposure without PNI. All the rats were observed closely during the initial 2 h recovery period and returned to housing in a central animal care facility. All animals were screened postoperatively for infections, weight loss, and any other disabilities. Additionally, 0.25% bupivacaine and 0.5%

lidocaine were used for analgesia for 48 h. One week later, all rats were sacrificed and the sciatic nerves of each rat were isolated and digested to harvest Schwann cells. Normal Schwann cells (NSCs) and activated Schwann cells (ASCs) were isolated and cultured from the sciatic nerves of the Sham group and the PNI group respectively. The cell culture medium included dulbecco's modified eagle medium/nutrient mixture f-12 (DMEM/F-12, Gibco, USA), fetal bovine serum (FBS, Gibco, USA) and antibiotic-antimycotic (AA, Gibco, USA). Differential adhesion method was used for the purification Schwann cell. The final Schwann cells purities reached 95% as confirmed by morphology and immunostaining of S100beta. At passage three, both ASCs and NSCs were used to detect the different changes in the genome (methylated DNA immunoprecipitation sequencing, MeDIP-seq) and proteome (tandem mass tags, TMT).

For the verification of Schwann cells, both ASCs and NSCs were seeded with 1000 cells per well on the Cell Culture Slides (Corning®, USA). After 3 days cultured, all cells were fixed with 4% paraformaldehyde solution (Santa Cruz, USA) and 5% bovine serum albumin (Sigma, USA), respectively. Then, the cells were stained with S100beta (ab52642, Abcam, USA) and Hoechst 33,342 (Thermo, USA) respectively. Finally, the fluorescent images were observed and captured using confocal laser scanning microscopy (LSM 780, Zeiss, Germany).

2.3. Methylated DNA immunoprecipitation sequencing

High-throughput methylated DNA immunoprecipitation Sequencing analysis was used to detect the different gene expression of ASCs and NSCs according to previous studies [22,23]. Briefly, DNA from each samples were purified and sonicated to produce DNA fragments (100–500 bp). Subsequently, sequencing adapters-ligated DNA and 5-methylcytosine antibody beads were immunoprecipitated. Quantitative real-time polymerase chain reaction was performed to amplify and verify the specificity of the immunoprecipitated fragments. Finally, DNA library quality control and sequencing run were processed by an Illumina HiSeq 2000 Sequencing System. Differentially expressed genes were selected (mean difference ≥20, $p < 0.05$).

2.4. Tandem mass tags labeling

Tandem Mass Tags (TMT) labeling analysis was used to detect the relative protein expression of each groups according to previous studies [24]. Briefly, three samples of PNI and Sham group (100 µg of each sample) were dissolved in 100 mM triethyl ammonium bicarbonate (TEAB), and incubated for 1 h. Then, the samples with iodoacetamide were incubated for 30 min at room temperature. After digested with trypsin and adjusted the pH, all samples were labeled with TMT six-plex

isobaric label reagent set (Thermo Fisher Scientific, USA). Differentially expressed proteins were screened (fold change ≥ 1.5 , $p < 0.05$).

2.5. Bioinformatic analysis

All differential expression genes (DEGs) and differential expression proteins (DEPs) in the peripheral nerve genome and proteome were identified. For further protein–protein interaction (PPI) in silico network analysis and statistical analysis of gene/protein expression, all DEGs/DEPs were imported into and Cytoscape (v3.7.1) for further analysis. For Gene Ontology (GO) analysis and the Kyoto Encyclopedia of Genes and Genomes (KEGG) analysis, all DEGs/DEPs were put into the DAVID (the Database for Annotation, Visualization and Integrated Discovery, <https://david.ncifcrf.gov/summary.jsp>, April 26, 2020).

2.6. Cellular uptake test

For the cellular uptake of exosomes (hTERT MSC Exosomes, ATCC, USA), both ASCs and NSCs were seeded with 500 cells per well on the Cell Culture Slides (Corning®, USA). After 3 days cultured in DMEM containing 10% FBS and 1% AA. Before cellular uptake, the concentration, size distribution, and diameter of exosomes were detected by the Nanosight system (NS300, Malvern, UK). The particles concentration and size distribution were measured by nanoparticle tracking analysis (v3.20 software). All exosomes were labeled with 1 mM Vybrant® CM-Dil solution (Invitrogen, USA). Then, the CM-Dil labeled exosomes were incubated with both ASCs and NSCs in serum-free DMEM at 37 °C for 0, 1, 2, 3, 4 h, respectively. After fixed with 4% paraformaldehyde solution (Santa Cruz, USA) and 5% BSA (Sigma, USA), the cells were stained with F-actin Alexa Fluor™ 488 Phalloidin (Invitrogen, A12379, USA) and Hoechst 33,342 (Thermo, USA) respectively. Finally, the fluorescent images were observed and captured using confocal laser scanning microscopy (LSM 780, Zeiss, Germany). All red area was imported into Image J (v1.48) for quantization.

2.7. Quantitative real-time RT-PCR

For qRT-PCR, both ASCs and NSCs were harvested in order to investigate whether gene expression difference according to above bioinformatic analysis. Briefly, All samples were performed on C1000 Touch™ Thermal Cycler using SYBR Green PCR Master Mix (Quanta bio, USA) to measure the gene expressions of Ras-related protein Rab-7a (RAB7A), ADP-ribosylation factor 6 (ARF6), Ras-related protein Rab-5A (RAB5A), Ras-related protein Rab-11 A (RAB11A), Transforming protein RhoA (RHOA), ADP-ribosylation factor 1 (ARF1), Dynamin-3 (DNM3), Proto-oncogene tyrosine-protein kinase Src (SRC), E3 ubiquitin-protein ligase NEDD4 (NEDD4), and Vacuolar protein sorting-associated protein 45 (VPS45). GAPDH was as an internal control. The primers are shown in Table 1. The relative quantification of the genes of interest was calculated using the 2- $\Delta\Delta C_t$ method.

Table 1
Information on primer sequences.

Gene	Product Length	Forward Primer	Reverse Primer	Reference
Rab7a	114	gggagactctggtgtggaa	accatcactccttggctcag	NM_023,950.3
ARF6	95	cagggtctgatctctgtggt	ctcatctcccggctcattgat	NM_024,152.2
Rab5a	143	ctggccaagaacggtatcat	aggacttgccttgccttgaa	NM_022692.1
Rab11a	118	ttgcaacaagaagcatccag	gcacctactgtccacagatag	NM_031,152.2
Rhoa	110	aaggaccagttcccagaggt	tgccagctgtgtccataa	NM_057,132.3
Arf1	96	gaagatgagetccagatgc	ccccagctgtctgtgattt	NM_022,518.3
Dnm3	83	tggagaggcaagtggagact	tggaattaggctcggatgc	NM_138538.1
Src	88	cttctctgtgaggagagtg	tttcacatttaggccccttg	NM_031977.1
Nedd4	100	catgtgtggtctggagatg	ccagaaccagtggatgacct	NM_012986.1
Vps45	140	tcagtgaacgaaacctgctg	cactaggcgaactcatcaa	NM_172072.2
GAPDH	85	tgccactcagaagactgtgg	ggatgcaggatgatgtct	NM_017,008.4

2.8. Statistical analysis

All data was presented as mean \pm SEM. The values of $P < 0.05$ was considered a statistically significant difference. GraphPad Prism statistical software (v8.0.2) was employed for data analysis. Comparisons between two groups were performed by the Student's t test.

3. Results

3.1. Endocytosis-related genes after PNI

After peripheral nerve injury, a total of 14,770 DEGs were identified using MeDIP-seq. The volcano plot is shown in Fig. 1A. The pink points were upregulated genes and blue points were downregulated genes. All 46 endocytosis-related DEGs (Inclusion criteria: mean difference ≥ 20 , $P < 0.05$) were crudely classified into six major groups according to the genomic architecture, including promoter (2.9%), intron (18.6%), exon (4.3%), downstream (2.9%), 3'utr (35.7%), and distal intergenic (35.7%) (Fig. 1B). The chromosomal distribution of these DEGs in peripheral nerve injury is shown in Fig. 1C. Furthermore, 46 endocytosis-related DEGs are shown in a heat map (Fig. 1D).

3.2. Endocytosis-related proteins after PNI

A total of 3249 differentially expression proteins were identified from the TMT labeling. The length of the peptide distribution in this study is shown in the Fig. 2A. The negative correlation between protein sequence coverage and protein mass is shown in Fig. 2B. The volcano plot is shown in Fig. 2C. The red points were upregulated proteins and green points were downregulated proteins. Among these proteins, 18 endocytosis-related DEPs were selected (Inclusion criteria: fold change ≥ 1.5 , $P < 0.05$) and shown in a heat map (Fig. 2D).

3.3. Bioinformatics analysis of endocytosis-related genes

Regarding the KEGG enrichment analysis of DEGs, the results of KEGG enrichment analysis showed that the DEGs of PNI were mainly enriched in Endocytosis pathway (Fig. 3A). The PPI network of DEGs of the peripheral nerve was performed by cytoscape and shown in Fig. 3B. The pink nodes were upregulated genes and blue nodes were downregulated genes. In addition, 9 core DEGs were chosen: *Rab7a*, *Afr6*, *Rab11a*, *Src*, *Rhoa*, *Rab5a*, *Arf1*, *Nedd4*, and *Dnm3*. The number of these core gene edges are shown in Fig. 3C.

GO enrichment analysis were presented in Fig. 3D. For biological processes (BP), DEGs of PNI were significantly enriched in vesicle-mediated transport (GO:0016,192), localization (GO:0051,179), transport (GO:0006810), macromolecule localization (GO:0033,036), and protein localization (GO:0008104). For molecular function (MF), DEGs of PNI were significantly enriched in purine ribonucleoside triphosphate binding (GO:0035,639), purine ribonucleotide binding (GO:0032,555), protein binding (GO:0005515), binding (GO:0005488), and small

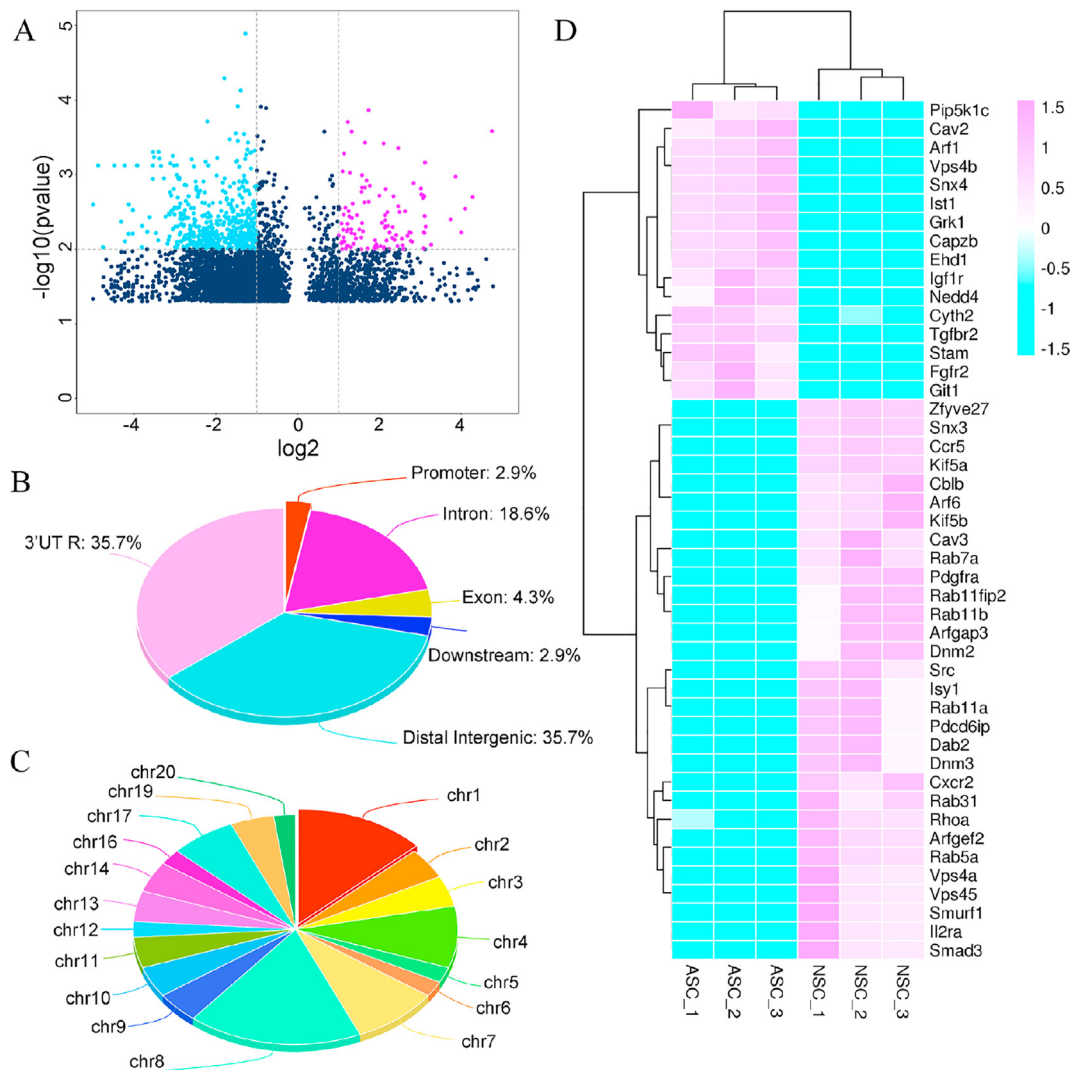


Fig. 1. Signatures of differential expression genes in PNI (A) Volcano plot for the differential expression genes (B) Differential expression genes were classified according their genomic architecture in PNI (C) Chromosome distribution showed the ratio of genes located at different chromosomes (D) Representative heatmap of the 46 endocytosis-related DEGs. PNI, peripheral nerve injury; DEGs, differential expression genes.

molecule binding (GO:0036,094). Regarding the cellular component (CC), DEGs of PNI were significantly enriched in vesicle (GO:0031,982), cytoplasmic vesicle (GO:0031,410), endosome (GO:0005768), whole membrane (GO:0098,805), and cytoplasm (GO:0005737).

3.4. Bioinformatics analysis of endocytosis-related proteins

Regarding the KEGG enrichment analysis of DEPs, the results of KEGG enrichment analysis showed that the DEPs of PNI were mainly enriched in Endocytosis pathway (Fig. 4A). The PPI network of 18 DEPs of the peripheral nerve was performed by cytoscape and shown in Fig. 4B. The orange nodes were upregulated genes and green nodes were down-regulated genes. In addition, 9 core DEPs were chosen: RAB7A, ARF6, A0A0G2JZR4, RAB5A, A0A0A0MY48, KINH, VPS45, ARFG3, and A0A0G2JSZ1. The number of these core gene edges are shown in Fig. 4C.

For the biological processes of GO enrichment analysis (Fig. 4D), DEPs of PNI were significantly enriched in protein transport (GO:0015,031), vesicle-mediated transport (GO:0016,192), transport (GO:0006810), regulation of signaling (GO:0023,051), and cellular

component organization (GO:0016,043). For molecular function, DEPs of PNI were significantly enriched in GTP binding (GO:0005525), protein binding (GO:0005515), binding (GO:0005488), GTPase activity (GO:0003924), and purine ribonucleoside triphosphate binding (GO:0035,639). Regarding the cellular component, DEPs of PNI were significantly enriched in cytoplasmic vesicle (GO:0031,410), endocytic vesicle (GO:0030,139), phagocytic vesicle (GO:0045,335), endosome (GO:0005768), and phagocytic vesicle membrane (GO:0030,670).

3.5. Identification of activated Schwann cells and normal Schwann cells

After surgery, all animal survival without complication. At passage three post isolation of cells, the morphology of ASCs and NSCs were similar to the spindle cells with long axons. Based on the immunocytochemical staining, both ASCs and NSCs expressed the peripheroneural marker S100beta (Fig. 5). All Schwann cells were prepared for methylated DNA immunoprecipitation sequencing and tandem mass tags labeling after immunofluorescence identification.

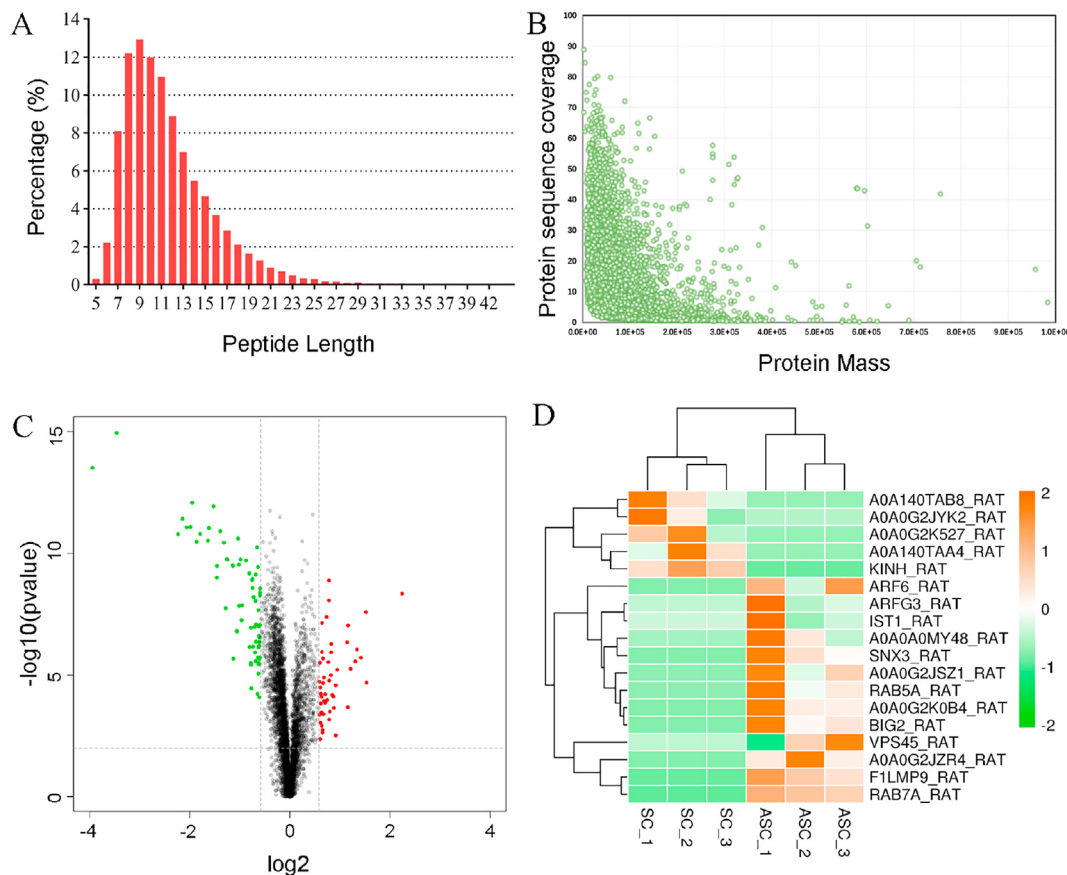


Fig. 2. Signatures of differential expression proteins in PNI (A) Peptide length distribution of differential expression proteins in PNI (B) The negative correlation between protein sequence coverage and protein mass (C) Volcano plot for the differential expression proteins (D) Representative heatmap of the 18 endocytosis-related DEPs. PNI, peripheral nerve injury; DEPs, differential expression proteins.

3.6. Activated Schwann cells showed higher cellular uptake ability than normal Schwann cells

The cellular uptake of exosomes (hTERT MSC Exosomes) into Schwann cells was observed and captured with confocal microscopy. The exosomes were labeled with CM-Dil (red), the cytoskeletal was labeled by F-actin/phalloidin (green) and the nuclei was labeled by Hoechst 33,342 (blue) (Fig. 6A). All cells were detected after coculture with exosomes for 0, 1, 2, 3, 4 h, respectively. For the exosomes, the diameter and particles concentration of exosomes were 141.7 nm and 2.97×10^7 particles/mL, respectively (Fig. 6 B and C). The size distribution of exosomes was 50–200 nm (Fig. 6D). In conclusion, the ASCs showed higher cellular uptake ability than NSCs from 1 to 4 h (Fig. 6E).

3.7. Pathway analysis of DEGs/DEPs targets

In the Endocytosis signaling pathway, markers with green background indicated the DEGs of PNI, while with yellow background indicated the common markers (including the DEGs and DEPs) of PNI (Fig. 7A). In addition, qRT-PCR was used to verify above endocytosis-related markers (*RAB7A*, *ARF6*, *RAB5A*, *RAB11A*, *RhoA*, *ARF1*, *DNM3*, *SRC*, *NEDD4*, and *VPS45*) in ASCs compared with NSCs. As shown in Fig. 7B, the expression of *RAB7A*, *ARF6*, *ARF1*, and *VPS45* was significantly increased in the ASCs compared to the NSCs. The expression of *RAB11A*, *DNM3* and *NEDD4* was significantly decreased in the ASCs

Group. For the expression of *RAB5A*, *RhoA* and *SRC*, there were no significant changes between two groups.

4. Discussion

Schwann cells, as one of the most common cells in the nervous system, participate in the development of nerves, regulation of homeostasis, activation and response after peripheral nerve injury [25]. Schwann cells have slow self-regulation and self-renewal ability and could secrete multiple factors and remyelination. Nerve injury is usually accompanied by the removal of myelin debris and the reconstruction of axons. Among them, endocytosis is one of the important functions of Schwann cells involved in the clearance of myelin. In this study, we first established a subacute model of peripheral nerve injury. Then, methylated DNA immunoprecipitation sequencing and tandem mass tags labeling were used to detect differential expression genes and proteins in the injured peripheral nerve. Approximately 46 endocytosis-related DEGs and 18 DEPs were screened out after PNI. After KEGG signaling pathway analysis, PPI network analysis, and GO analysis of these DEGs/DEPs, several common core markers were screened out. These targets may play a significant role in both slow recycling and ARF-6 dependent recycling of the endocytic signaling pathway.

Peripheral nerve injury can lead to great morbidity in those afflicted, ranging from sensory loss, motor loss, chronic pain, or a combination of deficits [26]. Due to the complex structure of nerve regeneration organs,

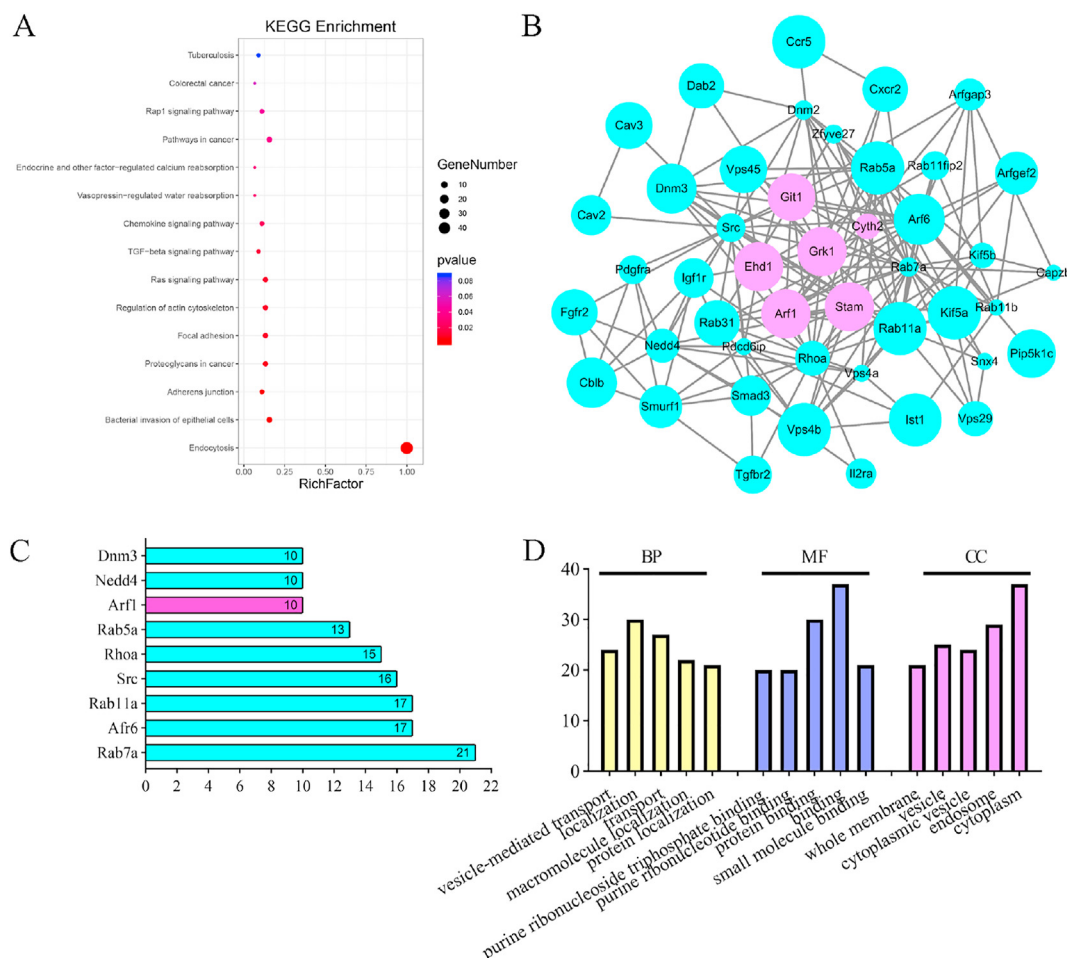


Fig. 3. Bioinformatics of the differential expression genes in PNI (A) Top 15 of KEGG pathway analysis of DEGs in PNI. The circles represent biological processes; The colour represents P value; The size of the circles indicate the rich factor in one pathway (B) PPI network of the DEGs in PNI. Pink represents the up-regulated genes and blue represents the down-regulated genes. The size of circles represents the P value of genes, larger nodes have lower P values (C) Core differential expression genes in PNI (D) GO analysis of differential expression genes in PNI. PNI, peripheral nerve injury; DEGs, differential expression genes; GO, gene ontology; KEGG, Kyoto Encyclopedia of Genes and Genomes; PPI, protein–protein interaction.

it is difficult to replicate in vitro. So far, in vitro research on nerve regeneration is very limited. This part of preclinical research is mainly conducted on animal models [27]. At present, the most commonly used experimental model is based on the injury of the sciatic nerve, the largest nerve trunk in mammals [28]. Among the various reasons that may explain the preponderancy of sciatic nerve injury employment, two are the most important: (i) the sciatic nerve is large and easy to operate; (ii) convenient surgical access; Moreover, the sought for data that can be comparable with previous studies, the very large majority of which have been carried out using the sciatic nerve injury model. Compared with peripheral nerve injury, there are many models of central nerve injury. Central nerve injury models are categorized based on the mechanism of injury into contusion, compression, distraction, dislocation, transection, or chemical models [29]. Although it is necessary to reach a consensus to clearly define the adequate ambits and the minimal reporting standards for pre-clinical use of different models, based on our current knowledge, it seems that no experimental model of nerve injury and regeneration has inherent advantages.

The endocytosis pathway is one of the important pathways for cells to take in nutrients or drugs, RNA and proteins, and resist parasites [30–33]. In the latest researches, some studies have shown that it also affects and regulates the synaptic activity of synaptic and membrane

recovery [34]. Most importantly, the release of neurotransmitters is achieved by fusing synaptic vesicles with the plasma membrane (endocytosis and exocytosis) [35]. Among them, various proteins and bioactive factors are involved in endocytosis, exocytosis, circulation, and degradation of neurotransmitters [36,37]. In the central nervous system (CNS), the exo- and endocytosis pathway are involved in the transmission of synaptic vesicles which store neurotransmitters, and in the peripheral nervous system (PNS), it also plays a role in the removal of myelin debris and regeneration of myelin [37]. Therefore, we focused on several important targets that affect the slow recycling and ARF-6 dependent recycling in the endocytosis signaling pathway. We tried to start with the corresponding targets in order to find the direction of remodeling and regeneration after peripheral nerve injury.

In this program, we identified the common targets (e.g. Rab7a, Afr6, and Rab5a, the gene name corresponding to the protein according to the Uniprot (<https://www.uniprot.org/>, 2020/04/15)) in the endocytosis pathway of Schwann cells after peripheral nerve injury through both genome and proteome. Previous studies have certified that the down-regulation of Rab8a/Rab11a can inhibit the transfer of vesicles, thereby reducing cell migration and triggering apoptosis of Schwann cells [38]. This is consistent with our research results. We found that the changes of Rab11a and Rab11 b together affect the formation and growth

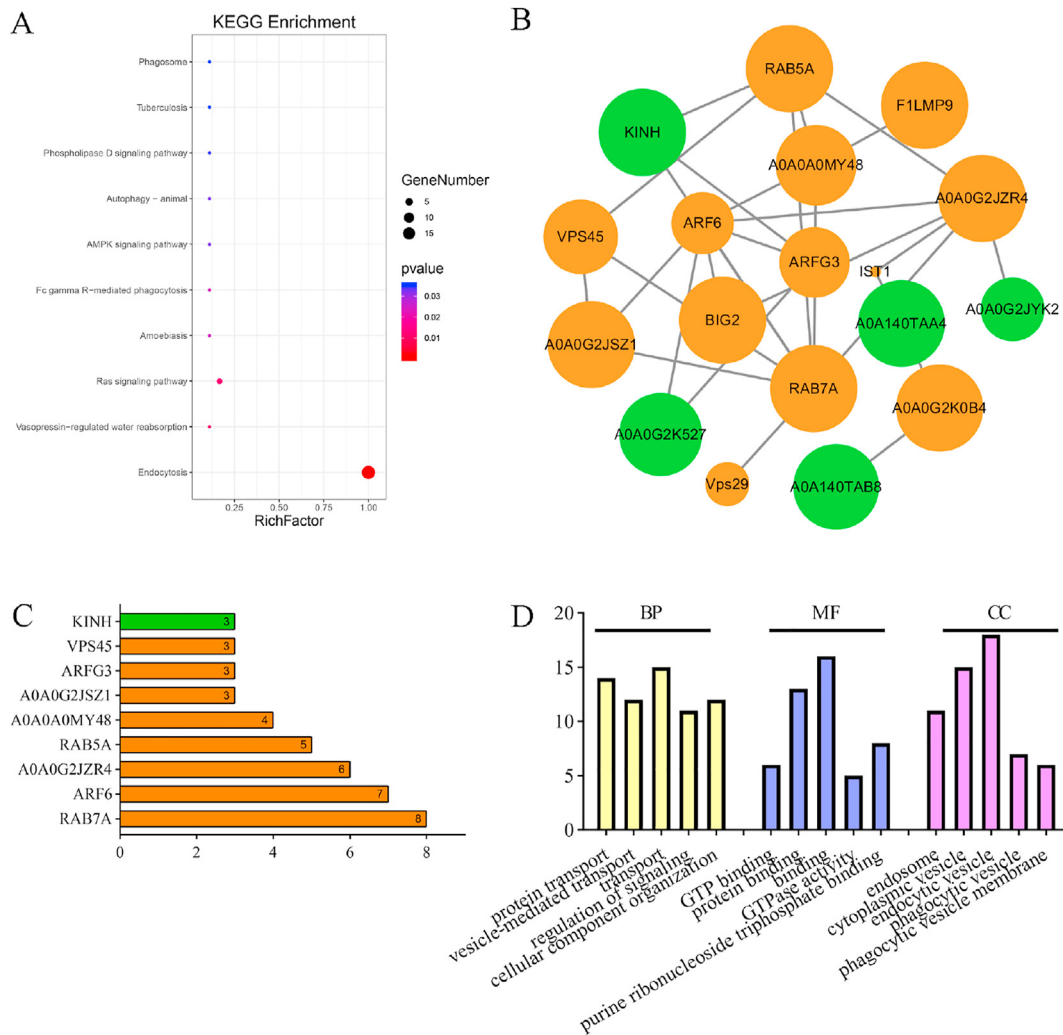


Fig. 4. Bioinformatics of the differential expression proteins in PNI (A) Top 10 of KEGG pathway analysis of DEPs in PNI. The circles represent biological processes; The colour represents P value; The size of the circles indicate the rich factor in one pathway (B) PPI network of the DEPs in PNI. Orange represents the up-regulated proteins and green represents the down-regulated proteins. The size of circles represents the P value of proteins, larger nodes have lower P values (C) Core differential expression proteins in PNI (D) GO analysis of differential expression proteins in PNI. PNI, peripheral nerve injury; DEPs, differential expression proteins; GO, gene ontology; KEGG, Kyoto Encyclopedia of Genes and Genomes; PPI, protein–protein interaction.

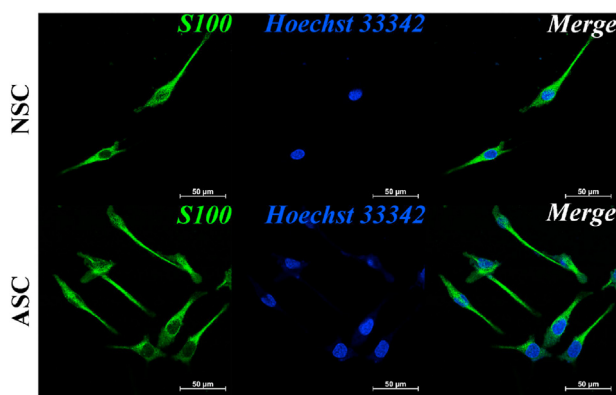


Fig. 5. Immunofluorescence staining of NSCs and ASCs. Schwann cells were labeled with S100 (Green) and the nucleus of Schwann cells was labeled with Hoechst 33,342 (Blue) by immunofluorescence. Scale bar: 50 μm. ASCs, Activated Schwann cells. NSCs, Normal Schwann cells.

of axons, and this change may be achieved by regulating the transfer of intracellular and extracellular vesicles. In addition, at the late stages of the endocytic signaling pathway, Rab7a controls the trafficking and signaling of neurotrophins and plays a special role in neuron migration and neurite outgrowth [39]. This was also verified in our experiments, and our results show that Rab7a plays an irreplaceable role at both gene and protein levels. In recent years, accumulating studies have reported the role of Arf6 plays pivotal roles in a variety of cellular events (autophagy, endocytosis, and exocytosis) [40–42]. Clathrin-mediated endocytosis regulated by Arf6 activation may be related to the up-regulation of upstream GTPase dynamin2 (Dyn2) expression [43]. In different critical processes of endocytosis (e.g. cytokinesis, cell motility), Arf6 may play multiple roles including regulation of intracellular signaling, lipid cargo, and regulation of cell membrane motion [44]. This is consistent with our previous conclusion that Arf6 could modify cell endocytosis and vesicle intracellular circulation.

Although there are significant discoveries related to the cellular endocytosis after peripheral nerve injury in these studies, there are also limitations. First, only eighteen rats, with small sample size, were sacrificed for research in this program. And rodents cannot represent all

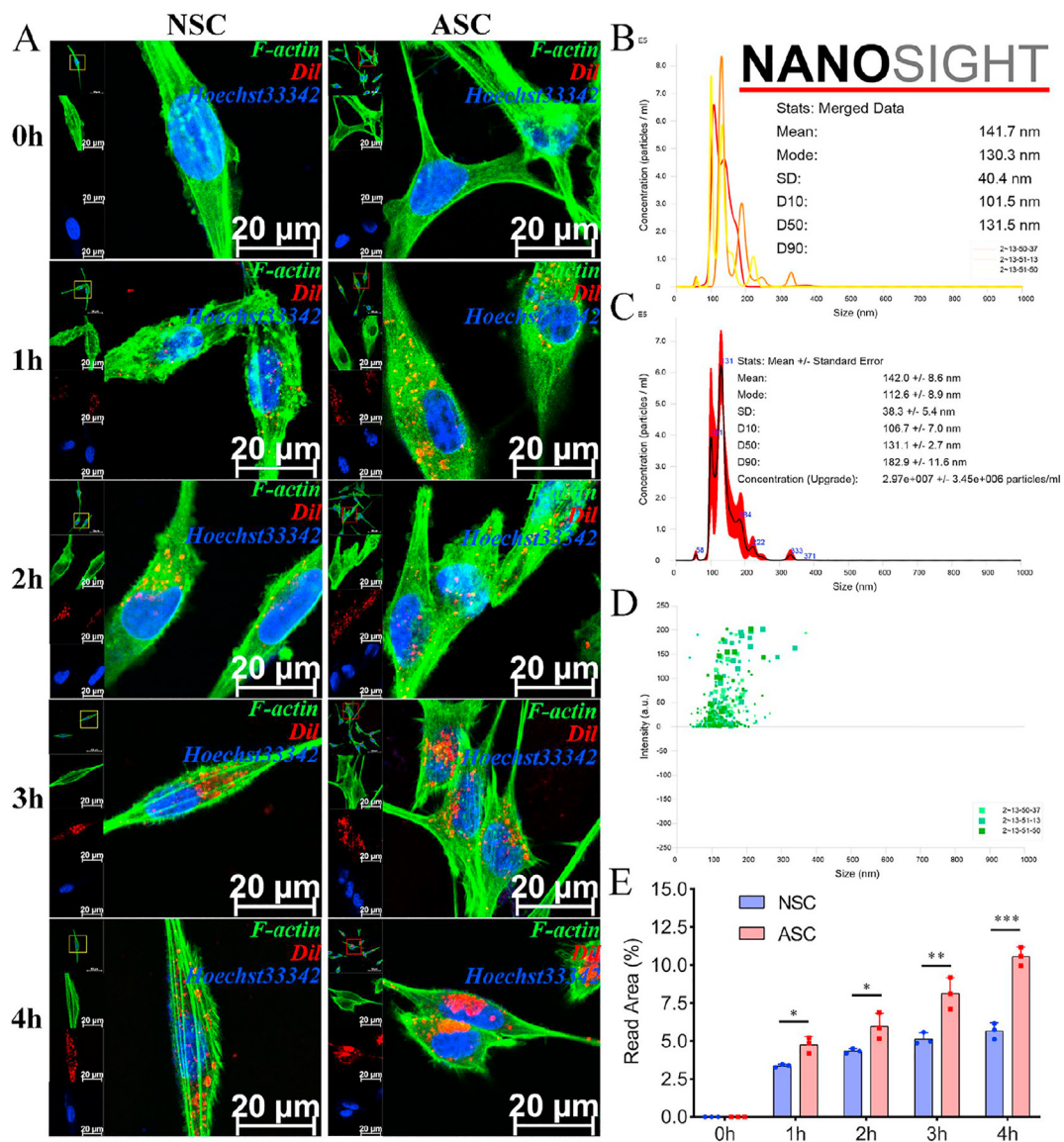


Fig. 6. The cellular uptake of exosomes into Schwann cells (A) The exosomes were labeled with CM-Dil (red), the cytoskeletal was labeled by F-actin/phalloidin (green) and the nuclei was labeled by Hoechst 33,342 (blue). All cells were detected after coculture with exosomes for 0, 1, 2, 3, 4 h, respectively. Scale bar: 20 μ m (B and C) The diameter and particles concentration of exosomes were 141.7 nm and 2.97×10^7 particles/mL, respectively (D) The size distribution of exosomes was 50–200 nm (E) The ASCs showed higher cellular uptake ability than NSCs from 1 to 4 h. ASCs, Activated Schwann cells. NSCs, Normal Schwann cells.

animals. In the future, large animals and even primates should be used more in the exploration of peripheral nerve injury. Second, the sciatic nerves were used to study in this program, while the sciatic nerves cannot represent all peripheral nerves. Also, Schwann cells are common but not the only cells in peripheral nerves, and more diverse cell research requires further exploration. Third, this study has not been verified from the cellular level, animal behavior or histology level, and there is still a large research space that requires more work. Fourth, compare with Schwann cells, macrophages also play a clear role in the fragments of cells and myelin [45]. Finally, since our team has previously analyzed changes at different time points (0, 3, 7 and 14 days) after peripheral nerve injury [46], this study only selected the single time point of 7 days

after sciatic nerve injury, we plan to incorporating more time points for research in the future.

5. Conclusion

In conclusion, this study reveals the endocytosis-related targets in the peripheral nerve system through genomics and proteomics analysis. We used MeDIP-seq, TMT labeling analysis, and bioinformatics to target the DEGs/DEPs after peripheral nerve injury. Genes or proteins changes of some common targets after PNI are preferred to be exo- or endocytosis biomarkers for nerve regeneration and axon remodeling. In addition, we verified that the higher cellular uptake activity of ASCs compared to

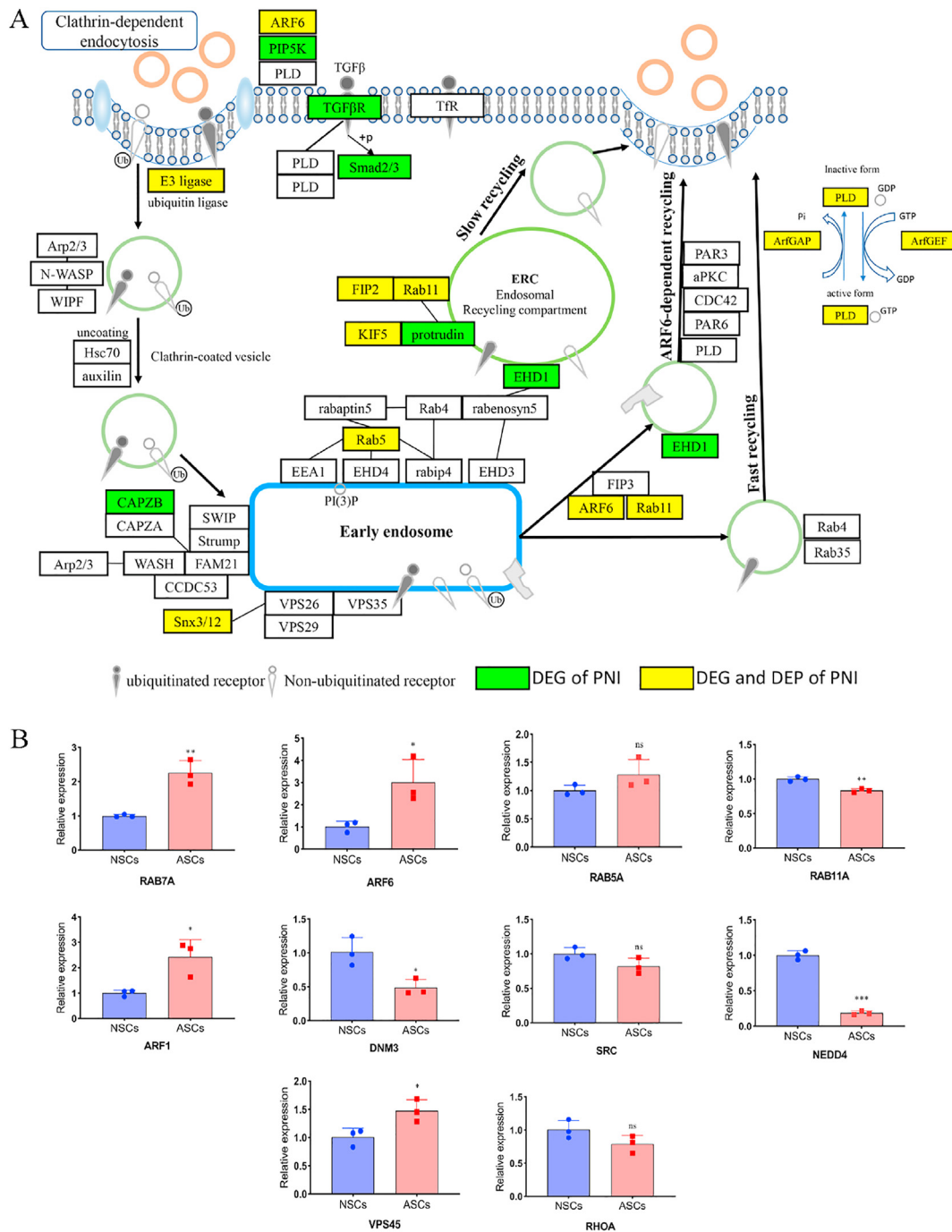


Fig. 7. Endocytosis pathway analysis of PNI (A) Green represents the markers detected by MeDIP-seq in PNI. Yellow represents the common marker detected by the MeDIP-seq and TMT labeling analysis. These markers may control the slow recycling and ARF6-dependent recycling after peripheral nerve injury (B) The relative expressions of *RAB7A*, *ARF6*, *RAB5A*, *RAB11A*, *RhoA*, *ARF1*, *DNM3*, *SRC*, *NEDD4*, and *VPS45* were determined by qRT-PCR in ASCs compared with NSCs. PNI, peripheral nerve injury; MeDIP-seq, methylated DNA immunoprecipitation sequencing. TMT, tandem mass tags. DEG, different expression gene. DEP, different expression protein. ASCs, Activated Schwann cells. NSCs, Normal Schwann cells.

NSCs may be caused by the up-regulation of *RAB7A*, *ARF6*, *ARF1*, *VPS45*, and down-regulation of *RAB11A*, *DNM3*, *NEDD4*. These results may provide novel insights for the removal of myelin debris and the regeneration of myelin in the subacute stage of nerve injury. Further explorations are required to validate the function and characters of these biomarkers.

Funding

This study was supported by grants from the State General Program National Natural Science Foundation of China (grant number: 81371957); Postgraduate Innovation Fund of '13th Five-Year comprehensive investment', Tianjin Medical University (grant number:

YJSCX201903). The authors Guidong Shi are funded by the China Scholarship Council, Qilu Hospital of Shandong university Orthopedic Scientific Research Foundation for the Young Scholars, and Tianjin Research Innovation Project for Postgraduate Students (grant number: 2019YJBS109).

Declaration of competing interest

The authors declare that there are no conflict of interests.

References

- [1] Fadia NB, Bliley JM. Long-gap peripheral nerve repair through sustained release of a neurotrophic factor in nonhuman primates 2020;12(527).
- [2] Fledrich R, Akkermann D, Schutzva V, Abdelal TA. NRG1 type I dependent autocrine stimulation of Schwann cells in onion bulbs of peripheral neuropathies 2019;10(1):1467.
- [3] Davies AJ, Kim HW, Gonzalez-Cano R, Choi J, Back SK, Roh SE, et al. Natural killer cells degenerate intact sensory afferents following nerve injury. *Cell* 2019;176(4): 716–28. e18. [eng].
- [4] Meyers EC, Kasliwal N. Enhancing plasticity in central networks improves motor and sensory recovery after nerve damage 2019;10(1):5782.
- [5] Inoue K. The function of microglia through purinergic receptors: neuropathic pain and cytokine release. *Pharmacol Ther* 2006;109(1–2):210–26 [eng].
- [6] Dong L, Li R, Li D, Wang B, Lu Y, Li P, et al. FGF10 enhances peripheral nerve regeneration via the preactivation of the PI3K/akt signaling-mediated antioxidant response. *Front Pharmacol* 2019;10:1224 [eng].
- [7] Yi S, Tang X, Yu J, Liu J, Ding F, Gu X. Microarray and qPCR analyses of wallerian degeneration in rat sciatic nerves. *Front Cell Neurosci* 2017;11:22 [eng].
- [8] Yu J, Gu X, Yi S. Ingenuity pathway analysis of gene expression profiles in distal nerve stump following nerve injury: insights into wallerian degeneration. *Front Cell Neurosci* 2016;10:274 [eng].
- [9] Fawcett JW, Keynes RJ. Peripheral nerve regeneration. *Annu Rev Neurosci* 1990; 13:43–60 [eng].
- [10] Namgung U. The role of Schwann cell-axon interaction in peripheral nerve regeneration. *Cells Tissues Organs* 2014;200(1):6–12 [eng].
- [11] Dong R, Liu Y. MSC-derived exosomes-based therapy for peripheral nerve injury. *A Novel Therap. Strateg.* 2019;2019:6458237.
- [12] Rotschenker S. Wallerian degeneration: the innate-immune response to traumatic nerve injury. *J Neuroinflammation* 2011;8:109 [eng].
- [13] Lopez-Guerrero JA, de la Nuez C, Praena B, Sanchez-Leon E, Krummenacher C, Bello-Morales R. Herpes simplex virus 1 spread in oligodendrocytic cells is highly dependent on MAL proteolipid. *J Virol* 2020;94(4) [eng].
- [14] Liu CY, Yin G, Sun YD, Lin YF, Xie Z, English AW, et al. Effect of exosomes from adipose-derived stem cells on the apoptosis of Schwann cells in peripheral nerve injury. *Stem Cell Res Ther* 2020; 26: 2020. p. 189–96. 2.
- [15] Ching RC, Wiberg M, Kingham PJ. Schwann cell-like differentiated adipose stem cells promote neurite outgrowth via secreted exosomes and RNA transfer. *Stem Cell Res Ther* 2018;9(1):266 [eng].
- [16] Weiss T, Taschner-Mandl S, Bileck A, Slany A, Kromp F, Rifatbegovic F, et al. Proteomics and transcriptomics of peripheral nerve tissue and cells unravel new aspects of the human Schwann cell repair phenotype. *Glia* 2016;64(12):2133–53 [eng].
- [17] Forese MG, Pellegatta M, Canevazzi P, Gullotta GS, Podini P, Rivellini C, et al. Prostaglandin D2 synthase modulates macrophage activity and accumulation in injured peripheral nerves. *Neurosci Lett* 2020; 68: 2020. p. 95–110. 1.
- [18] Brosius Lutz A, Chung WS. Schwann cells use TAM receptor-mediated phagocytosis in addition to autophagy to clear myelin in a mouse model of nerve injury. *Neurosci Lett* 2017; 38: 2017. p. e80. E8072.
- [19] Scheib JL, Hoke A. An attenuated immune response by Schwann cells and macrophages inhibits nerve regeneration in aged rats. *Neurobiol Aging* 2016;45: 1–9 [eng].
- [20] Church JS, Milich LM, Lerch JK, Popovich PG, McTigue DM. E6020, a synthetic TLR4 agonist, accelerates myelin debris clearance, Schwann cell infiltration, and remyelination in the rat spinal cord. *Glia* 2017;65(6):883–99 [eng].
- [21] Keilhoff G, Fansa H, Schneider W, Wolf G. In vivo predegeneration of peripheral nerves: an effective technique to obtain activated Schwann cells for nerve conduits. *J Neurosci Methods* 1999;89(1):17–24 [eng].
- [22] Zhou XH, Lin W, Ren YM, Liu S, Fan BY, Wei ZJ, et al. Comparison of DNA methylation in schwann cells before and after peripheral nerve injury in rats. *BioMed Res Int* 2017;2017:5393268 [eng].
- [23] Shi G, Zhou X, Wang X, Zhang X, Zhang P, Feng S. Signatures of altered DNA methylation gene expression after central and peripheral nerve injury. *J Cell Physiol* 2019.
- [24] Shi GD, Cheng X, Zhou XH, Fan BY, Ren YM, Lin W, et al. iTRAQ-based proteomics profiling of Schwann cells before and after peripheral nerve injury. *Iran. J. Basic Med. Sci.* 2018;21(8):832–41.
- [25] Zhou X, Shi G, Fan B, Cheng X, Zhang X, Wang X, et al. Polycaprolactone electrospun fiber scaffold loaded with iPSCs-NSCs and ASCs as a novel tissue engineering scaffold for the treatment of spinal cord injury. *Int J Nanomed* 2018;13: 6265–77 [eng].
- [26] Sullivan R, Dailey T, Duncan K, Abel N, Borlongan CV. Peripheral nerve injury: stem cell therapy and peripheral nerve transfer. *Int J Mol Sci* 2016;17(12) [eng].
- [27] Geuna S, Raimondo S, Ronchi G, Di Scipio F, Tos P, Czaja K, et al. Chapter 3: histology of the peripheral nerve and changes occurring during nerve regeneration. *Int Rev Neurobiol* 2009;87:27–46 [eng].
- [28] Geuna S. The sciatic nerve injury model in pre-clinical research. *J Neurosci Methods* 2015;243:39–46 [eng].
- [29] Cheriyan T, Ryan DJ, Weinreb JH, Cheriyan J, Paul JC, Lafage V, et al. Spinal cord injury models: a review. *Spinal Cord* 2014;52(8):588–95.
- [30] Magez S, Pinto Torres JE, Obishakin E, Radwanska M. Infections with extracellular trypanosomes require control by efficient innate immune mechanisms and can result in the destruction of the mammalian humoral immune system. *Front Immunol* 2020;11:382 [eng].
- [31] Knapp O, Benz R. Membrane activity and channel formation of the adenylate cyclase toxin (CyaA) of bordetella pertussis in lipid bilayer membranes 2020;12(3).
- [32] Qian ZM, Li H, Sun H, Ho K. Targeted drug delivery via the transferrin receptor-mediated endocytosis pathway. *Pharmacol Rev* 2002;54(4):561–87 [eng].
- [33] Wickens JM, Alsaab HO, Kesharwani P, Bhise K, Amin M, Tekade RK, et al. Recent advances in hyaluronic acid-decorated nanocarriers for targeted cancer therapy. *Drug Discov Today* 2017;22(4):665–80 [eng].
- [34] Gaffield MA, Romberg CF, Betz WJ. Live imaging of bulk endocytosis in frog motor nerve terminals using FM dyes. *J Neurophysiol* 2011;106(2):599–607 [eng].
- [35] Hoopmann P, Punge A, Barysch SV, Westphal V, Buckers J, Opazo F, et al. Endosomal sorting of readily releasable synaptic vesicles. *Proc Natl. Acad. Sci. U.S.A* 2010;107(44):19055–60 [eng].
- [36] Rudolf R, Straka T. Nicotinic acetylcholine receptor at vertebrate motor endplates: endocytosis, recycling, and degradation. *Neurosci Lett* 2019;711:134434 [eng].
- [37] Jin Y, Seo KH, Ko HM, Jung TW, Chung YH, Lee JH, et al. Various approaches for measurement of synaptic vesicle endocytosis at the central nerve terminal. *Arch Pharm Res (Seoul)* 2019;42(6):455–65 [eng].
- [38] Zhu H, Xue C, Xu X, Guo Y, Li X, Lu J, et al. Rab8a/Rab11a regulate intercellular communications between neural cells via tunneling nanotubes. *Cell Death Dis* 2016; 7(12):e2523 [eng].
- [39] Romano R, Rivellini C, De Luca M, Tonlorenzi R, Beli R, Manganelli F, et al. Alteration of the late endocytic pathway in Charcot-Marie-Tooth type 2B disease. 2020.
- [40] Kinoshita-Kawada M, Hasegawa H, Hongu T, Yanagi S, Kanaho Y, Masai I, et al. A crucial role for Arf6 in the response of commissural axons to Slit1. *Neuron* 2019. 3.
- [41] Lin YC, Ohbayashi N, Hongu T, Katagiri N, Funakoshi Y, Lee H. Arf6 in lymphatic endothelial cells regulates lymphangiogenesis by controlling directional cell migration 2017;7(1):11431.
- [42] Castillo-Badillo JA. SRRF-stream imaging of optogenetically controlled furrow formation shows localized and coordinated endocytosis and exocytosis mediating membrane remodeling 2020;9(4):902–19.
- [43] Okada R, Yamauchi Y, Hongu T, Funakoshi Y, Ohbayashi N, Hasegawa H, et al. Activation of the small G protein Arf6 by Dynamin2 through guanine nucleotide exchange factors in endocytosis. *Sci Rep* 2015;5:14919 [eng].
- [44] Schweitzer JK, Sedgwick AE, D'Souza-Schorey C. ARF6-mediated endocytic recycling impacts cell movement, cell division and lipid homeostasis. *Semin Cell Dev Biol* 2011;22(1):39–47 [eng].
- [45] Faroni A, Mobasser SA, Kingham PJ, Reid AJ. Peripheral nerve regeneration: experimental strategies and future perspectives. *Adv Drug Deliv Rev* 2015;82-83: 160–7 [eng].
- [46] Pan B, Zhou HX, Liu Y, Yan JY, Wang Y, Yao X, et al. Time-dependent differential expression of long non-coding RNAs following peripheral nerve injury. *Int J Mol Med* 2017;39(6):1381–92.